

# Many-Particle and Many-Hole States in Neutron-Rich Ne Isotopes Related to Broken N=20 Shell Closure

Masaaki KIMURA<sup>1</sup> and Hisashi HORIUCHI<sup>2</sup>

<sup>1</sup>*RI-beam Science Laboratory, RIKEN (The Institute of Physical and Chemical Research), Wako, Saitama 351-0198, Japan.*

<sup>2</sup>*Department of Physics, Kyoto University, Kitashirakawa, Kyoto 606-8502, Japan*

## Abstract

The low-lying level structures of <sup>26</sup>Ne, <sup>28</sup>Ne and <sup>30</sup>Ne which are related to the breaking of the N=20 shell closure have been studied by the framework of the deformed-basis antisymmetrized molecular dynamics plus generator coordinate method using Gogny D1S force. The properties of the many-particle and many-hole states are discussed as well as that of the ground band. We predict that the negative-parity states in which neutrons are promoted into *pf*-orbit from *sd* orbit have the small excitation energy in the cases of <sup>28</sup>Ne and <sup>30</sup>Ne which, we regard, is a typical phenomena accompanying the breaking of N=20 shell closure. It is also found that the neutron *4p4h* structure of <sup>30</sup>Ne appears in low excitation energy which contains  $\alpha+^{16}\text{O}$  correlations.

## §1. Introduction

In these years, many experimental and theoretical efforts to investigate the properties of nuclei away from the stability valley have shown the variety of the nuclear binding systems which is beyond our standard understanding of the nuclear properties established in the study of the stable nuclei. The discovery of the neutron-halo phenomenon<sup>1)</sup> proved that the basic concept of the density saturation does not hold near the neutron drip-line. Another important concept of the shell structure and the magic number is also under the reconsideration because of their rearrangement in neutron-rich nuclei which is deduced from the breaking of the neutron shell closure in neutron-rich N=20 isotones.

The breaking of the N=20 shell closure in neutron-rich nuclei was firstly pointed out from the observation of the anomalous ground state spin of  $^{31}\text{Na}$ <sup>2)</sup> associated with the prolate deformation. Theoretically, it was suggested that the large deformation which is caused by the promotion of the neutrons from the *sd*-shell to *f*-shell possibly overcomes the N=20 shell effect in the neutron-rich N=20 isotones such as  $^{31}\text{Na}$  and  $^{32}\text{Mg}$ .<sup>3)</sup> The shell model studies<sup>4)-6)</sup> also support the neutron promotion into *pf*-shell and a striking result was given in  $^{32}\text{Mg}$ <sup>7)</sup> that neutron *2p2h* configuration (two holes in the *sd* shell and two particles in the *pf* shell) dominate the ground state of  $^{32}\text{Mg}$  and the large  $B(E2; 0_1^+ \rightarrow 2_1^+)$  due to the large deformation was predicted. Since the first observation of the  $B(E2; 0_1^+ \rightarrow 2_1^+)$  value in  $^{32}\text{Mg}$ <sup>8)</sup> which confirmed the shell model prediction, many experimental and theoretical studies have been devoted to  $Z \sim 10$  and  $N \sim 20$  nuclei.<sup>9)-24)</sup> And nowadays, the systematic large deformation and breaking of the N=20 shell closure are theoretically expected in the ground states of  $^{28-32}\text{Ne}$ ,  $^{29-33}\text{Na}$  and  $^{28-34}\text{Mg}$  and experimentally investigated in  $^{32,34}\text{Mg}$ . Recently, a new NN effective interaction which has a stronger  $(\sigma \cdot \sigma)(\tau \cdot \tau)$  term was suggested to explain the drastic change of the location of the neutron drip-line from oxygen isotopes to fluorine isotopes based on the monte carlo shell model study.<sup>15)</sup> They argued that the extension of the neutron drip-line in F isotopes is caused by the mixing of the neutron *0p0h*, *2p2h* and *4p4h* configurations which is driven not by the deformation but by the stronger  $(\sigma \cdot \sigma)(\tau \cdot \tau)$  interaction.

However, the experimental and theoretical information of low-lying states of neutron-rich isotopes is not enough yet. Especially, negative-parity states of even-even nuclei are not still confirmed in experiments<sup>18),24)</sup> and only little theoretical study has been made.<sup>6)</sup> The neutron *2p2h* dominance in the ground states of neutron-rich N=20 isotones implies that one or three neutrons can be easily promoted into *pf*-shell with small excitation energy which leads to the existence of the low-lying negative-parity states. Indeed, the shell model study<sup>6)</sup> has shown the possible existence of the low-lying neutron  $1\hbar\omega$  and  $3\hbar\omega$  states in

this mass region. Furthermore, the parity of the ground state of even-odd nuclei  $^{33}\text{Mg}$  is identified to be the positive<sup>25),26)</sup> which means the neutron  $1\hbar\omega$  structure of the ground state. Therefore it is of importance to study negative-parity states for understanding the structure of neutron-rich  $N\sim 20$  nuclei. In the same sense, the excited positive-parity bands which will have the neutron  $0p0h$  and  $4p4h$  structures dominantly are also important. Especially, in the case of the  $4p4h$  structure, due to the presence of the four neutrons in the  $pf$ -shell, the protons which are almost frozen in the ground state might be activated. Actually, we will show that the ( $\alpha+^{16}\text{O}$ +valence-neutrons type) cluster-like correlations can exist in the neutron  $4p4h$  structure of  $^{30}\text{Ne}$  which appears in rather low energy region.

The purposes of this article is to provide theoretical information on the properties of the negative-parity states and the excited bands of the positive-parity of the even-even Ne isotopes to understand the structure of the neutron-rich  $sd$ -shell nuclei around the broken  $N=20$  shell closure. The low-lying level structures of  $^{26}\text{Ne}$ ,  $^{28}\text{Ne}$  and  $^{30}\text{Ne}$  are discussed by using the deformed-basis AMD+GCM framework (deformed-basis antisymmetrized molecular dynamics plus generator coordinate method). The deformed-basis AMD framework has now been confirmed to describe well the mean-field like the Hartree-Fock method in addition to the ability of describing well the cluster structure. Since in AMD the energy variation is made after parity projection, the AMD can describe negative parity states which almost all Hartree-Fock calculations cannot treat. The use of AMD also enables us to study the possible existence of the  $\alpha+^{16}\text{O}$ +valence-neutrons type structure in neutron-rich Ne isotopes. Since the low-lying states of  $^{20}\text{Ne}$  have the  $\alpha+^{16}\text{O}$  cluster structure, the cluster correlation may survive even in the neutron-rich isotopes, like the case of neutron-rich Be isotopes which inherit the cluster structure of  $^8\text{Be}$ . It will be shown that the excitation energy of the negative-parity states becomes lower around  $N=20$  because of the breaking of the  $N=20$  shell closure and the  $\alpha+^{16}\text{O}$  cluster correlations appears in the positive-parity  $4p4h$  states.

The contents of this article is as follows. In the next section, the theoretical framework of the deformed-basis AMD is briefly explained. In the section 3, the obtained energy curves and level schemes are discussed. The  $E2$  transition probabilities are also studied. The density distribution and the possible existence of the cluster core in the ground and excited states of  $^{26}\text{Ne}$ ,  $^{28}\text{Ne}$  and  $^{30}\text{Ne}$  are examined. In the last section, we summarize this work.

## §2. Theoretical Framework

In this section, the framework of the deformed-basis AMD+GCM is explained briefly. For more detailed explanation of the framework of the deformed-basis AMD, readers are referred to references.<sup>27),28)</sup> The intrinsic wave function of the system with mass  $A$  is given

by a Slater determinant of single-particle wave packets  $\varphi_i(\mathbf{r})$ ;

$$\Phi_{int} = \frac{1}{\sqrt{A!}} \det\{\varphi_1, \varphi_2, \dots, \varphi_A\}, \quad (2.1)$$

$$\varphi_i(\mathbf{r}) = \phi_i(\mathbf{r})\chi_i\xi_i, \quad (2.2)$$

where the single-particle wave packet  $\varphi_i$  consists of the spatial  $\phi_i$ , spin  $\chi_i$  and isospin  $\xi_i$  parts. Deformed-basis AMD employs the triaxially deformed Gaussian centered at  $\mathbf{Z}_i$  as the spatial part of the single-particle wave packet.

$$\begin{aligned} \phi_i(\mathbf{r}) &\propto \exp\left\{-\sum_{\sigma=x,y,z} \nu_\sigma (r_\sigma - Z_{i\sigma})^2\right\}, \\ \chi_i &= \alpha_i\chi_\uparrow + \beta_i\chi_\downarrow, \quad |\alpha_i|^2 + |\beta_i|^2 = 1 \\ \xi_i &= \textit{proton} \quad \text{or} \quad \textit{neutron}. \end{aligned} \quad (2.3)$$

Here, the complex number parameter  $\mathbf{Z}_i$  which represents the center of the Gaussian in the phase space takes independent value for each nucleon. The width parameters  $\nu_x, \nu_y$  and  $\nu_z$  are real number parameters and take independent values for  $x, y$  and  $z$  directions, but are common to all nucleons. Spin part  $\chi_i$  is parametrized by  $\alpha_i$  and  $\beta_i$  and isospin part  $\xi_i$  is fixed to up (proton) or down (neutron).  $\mathbf{Z}_i, \nu_x, \nu_y, \nu_z$  and  $\alpha_i, \beta_i$  are the variational parameters and optimized by the method of frictional cooling. The advantage of the triaxially deformable single-particle wave packet is that it makes possible to describe the cluster-like structure and deformed mean-field structure within a single framework which discussed in reference.<sup>28)</sup>

As the variational wave function, we employ the parity projected wave function as in the same way as many other AMD studies

$$\Phi^\pm = P^\pm \Phi_{int} = \frac{(1 \pm P_x)}{2} \Phi_{int}, \quad (2.4)$$

here  $P_x$  is the parity operator and  $\Phi_{int}$  is the intrinsic wave function given in Eq(2.1). Parity projection makes possible to determine the different structure of the intrinsic state for the different parity states.

Hamiltonian used in this study is as follows;

$$\hat{H} = \hat{T} + \hat{V}_n + \hat{V}_c - \hat{T}_g, \quad (2.5)$$

where  $\hat{T}$  and  $\hat{T}_g$  are the total kinetic energy and the energy of the center-of-mass motion, respectively. We have used the Gogny force with D1S parameter set as an effective nuclear force  $\hat{V}_n$ . Coulomb force  $\hat{V}_c$  is approximated by the sum of seven Gaussians. The energy variation is made under a constraint on the nuclear quadrupole deformation by adding to

$\hat{H}$  the constraint potential  $V_{cnst} = v_{cnst}(\langle\beta\rangle^2 - \beta_0^2)^2$  with a large positive value for  $v_{cnst}$ . At the end of the variational calculation, the expectation value of  $V_{cnst}$  should be zero in principle and in the practical calculation, we confirm it is less than 0.1keV. The optimized wave function is denoted by  $\Phi^\pm(\beta_0)$ . Here it should be noted that this constraint does not refer to the deformation parameter  $\gamma$ , which means that  $\Phi^\pm(\beta_0)$  with positive  $\beta_0$  can be not only prolate but also oblate.

From the optimized wave function, we project out the eigenstate of the total angular momentum  $J$ ,

$$\Phi_{MK}^{J\pm}(\beta_0) = P_{MK}^J \Phi^\pm(\beta_0) = P_{MK}^{J\pm} \Phi_{int}(\beta_0). \quad (2.6)$$

Here  $P_{MK}^J$  is the total angular momentum projector. The integrals over the three Euler angles included in the  $P_{MK}^J$  are evaluated by the numerical integration.

Furthermore, we superpose the wave functions  $\Phi_{MK}^{J\pm}$  which have the same parity and the angular momentum but have different value of deformation parameter  $\beta_0$  and  $K$ . Thus the final wave function of the system becomes as follows;

$$\Phi_n^{J\pm} = c_n \Phi_{MK}^{J\pm}(\beta_0) + c'_n \Phi_{MK'}^{J\pm}(\beta'_0) + \dots, \quad (2.7)$$

where other quantum numbers except total angular momentum and parity are represented by  $n$ . The coefficients  $c_n, c'_n, \dots$  are determined by the Hill-Wheeler equation,

$$\delta(\langle\Phi_n^{J\pm}|\hat{H}|\Phi_n^{J\pm}\rangle - \epsilon_n \langle\Phi_n^{J\pm}|\Phi_n^{J\pm}\rangle) = 0. \quad (2.8)$$

### §3. Low-lying level structure of neutron-rich Ne isotopes

We have studied low-lying level schemes of the neutron-rich Ne isotopes,  $^{26}\text{Ne}$ ,  $^{28}\text{Ne}$  and  $^{30}\text{Ne}$  to study the change of the shell structure toward  $N=20$  and the mechanism of the nuclear excitation in these isotopes. For the positive-parity levels, the possible existence of the  $\alpha+^{16}\text{O}$  core is also examined.

Before the discussion on the obtained results, we explain the analysis of the obtained wave function and the notations used in this study to clarify our discussions. In this study, the single-particle structure of obtained wave function is analyzed by constructing the Hartree-Fock single-particle Hamiltonian from the obtained AMD wave function<sup>29)</sup> is as follows.

When the optimized wave function  $\Phi^\pm = P^\pm \frac{1}{\sqrt{A!}} \det\{\varphi_1, \varphi_2, \dots, \varphi_A\}$  is given, we calculate the orthonormalized basis  $\phi_\alpha$  which is a linear combination of the single-particle wave packets  $\varphi_i$ ,

$$\phi_\alpha = \frac{1}{\sqrt{\mu_\alpha}} \sum_{i=1}^A c_{i\alpha} \varphi_i. \quad (3.1)$$

Here,  $\mu_\alpha$  and  $c_{i\alpha}$  are the eigenvalue and eigenvector of the overlap matrix  $B_{ij} \equiv \langle \varphi_i | \varphi_j \rangle$ ,

$$\sum_{j=1}^A B_{ij} c_{j\alpha} = \mu_\alpha c_{i\alpha}, \quad (3.2)$$

and it is clear that  $\phi_\alpha$  is orthonormalized from this relation. Using this basis set of  $\phi_\alpha$ , we calculate the Hartree-Fock single-particle Hamiltonian  $h_{\alpha\beta}$  which is defined as,

$$\begin{aligned} h_{\alpha\beta} \equiv & \langle \phi_\alpha | \hat{t} | \phi_\beta \rangle + \sum_{\gamma=1}^A \langle \phi_\alpha \phi_\gamma | \hat{v}_{Gogny} + \hat{v}_{Coulomb} | \phi_\beta \phi_\gamma - \phi_\gamma \phi_\beta \rangle \\ & + \frac{1}{2} \sum_{\gamma\delta} \langle \phi_\gamma \phi_\delta | \phi_\alpha^* \phi_\beta \frac{\partial \hat{v}_{Gogny}}{\partial \rho} | \phi_\delta \phi_\rho - \phi_\rho \phi_\delta \rangle, \end{aligned} \quad (3.3)$$

where  $\hat{t}$ ,  $\hat{v}_{Gogny}$  and  $\hat{v}_{Coulomb}$  denote the kinetic operator, the Gogny force, and the Coulomb potential.  $\partial \hat{v}_{Gogny} / \partial \rho$  denotes the derivative of the density dependent term of the Gogny force.

By the diagonalization of  $h_{\alpha\beta}$ , we obtain the single-particle energy  $\epsilon_s$  and single-particle wave function  $\tilde{\phi}_s$ .

$$\sum_{\beta=1}^A h_{\alpha\beta} f_{\beta s} = \epsilon_s f_{\alpha s}, \quad (3.4)$$

$$\tilde{\phi}_s = \sum_{\alpha=1}^A f_{\alpha s} \phi_\alpha. \quad (3.5)$$

We note that the single-particle energy  $\epsilon_s$  and wave function  $\tilde{\phi}_s$  are obtained for occupied states but not for unoccupied states from this method. Furthermore, since the actual variational calculation is made after the parity projection (the superposition of the two Slater determinants), it does not allow the naive interpretation of  $\phi^\pm(\beta_0)$  by the single-particle picture. However, the single-particle structure obtained by this method is useful to understand the particle-hole structure of the obtained wave function. From the parity  $\pi_s^\pm = \langle \tilde{\phi}_s | P^\pm | \tilde{\phi}_s \rangle$  and the the angular momentum  $\langle \tilde{\phi}_s | \hat{j}_z | \tilde{\phi}_s \rangle$  in the intrinsic frame, we have judged the particle-hole structure. From this analysis, we find that the obtained wave functions have various single-particle structure. For example, in the case of the positive-parity states of  $^{30}\text{Ne}$ , neutron  $0p0h$ ,  $2p2h$  and  $4p4h$  structures with respect to  $N=20$  appear in the low-lying states. When protons are excited, proton  $2p0h$ ,  $3p1h$  and  $4p2h$  structures with respect to  $Z=8$  will be combined with the neutron  $ph$  structures. For the convenience, in the following, ‘ $mpnh$  structure’ denotes the neutron  $ph$  structure. When we need to distinguish it from that of protons, it will be written explicitly.

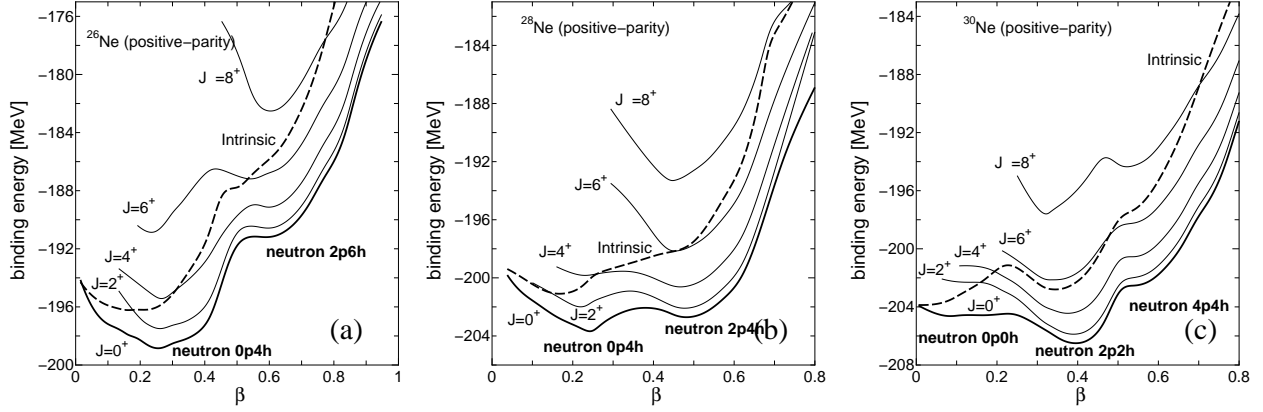


Fig. 1. Obtained energy curves of the positive parity states of  $^{26}\text{Ne}$  (a),  $^{28}\text{Ne}$  (b) and  $^{30}\text{Ne}$  (c). In each panel, the energies of the parity projected intrinsic state (dashed line), the parity and angular momentum projected states are plotted as the functions of the matter quadrupole deformation parameter  $\beta$ .

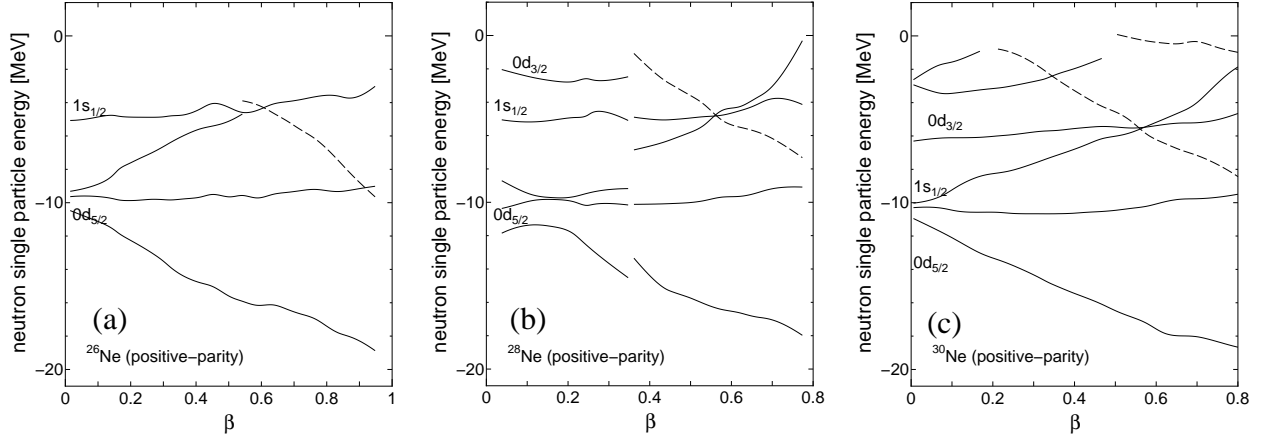


Fig. 2. The neutron single particle energies of  $^{26}\text{Ne}$  (a),  $^{28}\text{Ne}$  (b) and  $^{30}\text{Ne}$  (c) obtained from the intrinsic wave functions on the positive-parity energy curves. The positive (negative) parity single particle orbits are plotted by the solid (dashed) lines. Each single particle orbits are occupied by two neutrons.

### 3.1. Energy curves

The energy curves as function of the matter quadrupole deformation parameter  $\beta$  obtained before and after the angular momentum projection are shown in figure 1 for positive-parity states. The angular-momentum projected energy curve of the positive-parity state of  $^{30}\text{Ne}$  (figure 1 (c)) has an energy minimum around  $\beta \sim 0.4$  in each spin state. The energy gain of this deformed state is due to the restoration of the rotational symmetry and it amounts to about 5MeV in the case of the  $J^\pi=0^+$  state. This deformed minimum state has a neutron  $2p2h$  structure. The neutron single-particle energies of  $^{30}\text{Ne}$  are plotted as functions of deformation in figure 2 (c). From  $\beta=0$  to  $\beta=0.2$ , all neutrons are almost frozen

in the  $N=20$  shell closure. This inactivity of neutrons explains the absence of the  $6^+$  and  $8^+$  state in this region, since only two protons in  $sd$ -shell contribute to the total spin of the system. From  $\beta=0.2$  to  $\beta=0.5$ , two neutrons are promoted into the  $pf$ -shell ( $2p2h$ ) and the system is most deeply bound. The largely deformed state ( $\beta > 0.5$ ) has a  $4p4h$  structure in which four neutrons are promoted into the  $pf$ -shell. This state has not been discussed in detail in other model studies. One of the reason may be that the stability of the mean-field structure of this state is doubtful. Indeed, in our result, this state does not appear as a local minimum on the energy curve, but as a shoulder around  $\beta=0.5$ . However, when we superpose the wave functions on the energy curve, this state contributes to the  $K^\pi=0_3^+$  band and is stabilized through the orthogonalisation against the lower two bands. The parity projection before variation also helps to lower the energy of the  $4p4h$  structure. The energy of this state is lowered by about 2MeV by the parity projection, while  $0p0h$  and  $2p2h$  structure is not so affected (less than 1MeV). Note that the  $4p4h$  state has a parity asymmetric intrinsic density distribution. This asymmetry is the reason why the energy of the  $4p4h$  structure is lowered by the parity projection. Furthermore, the proton density distribution implies the possible existence of a  $\alpha+^{16}\text{O}$  cluster structure. Indeed, the overlap between the proton wave function of this state and that of the  $^{20}\text{Ne}$  which has an  $\alpha+^{16}\text{O}$  cluster structure is quite large and it amounts to about 80%. Therefore, the interpretation of this state by the  $\alpha+^{16}\text{O}$ +valance-neutron models will be efficient. In the present calculation, we did not find other state which has the apparent  $\alpha+^{16}\text{O}$ +valance-neutrons-like density distribution. The overlap of the proton wave function with that of  $^{20}\text{Ne}$  wave function is largest in this state, and it decreases in  $^{28}\text{Ne}$  and  $^{26}\text{Ne}$  as neutron number decreases. The existence of the  $0p0h$ ,  $2p2h$  and  $4p4h$  structure within small excitation energy (they lie within about 5MeV measured from the lowest  $2p2h$  structure) means the softness of the neutrons in the  $0d_{3/2}$  orbit of this nucleus. Namely, it does not cost much energy to promote neutrons from the shell which originates in the spherical  $0d_{3/2}$  shell into the higher shell which originates in the spherical  $pf$ -shell. It can be attributed to the large deformation caused by the neutron excitation, the restoration of the rotational symmetry and the reduced  $N=20$  energy gap owes to the excess of neutron.

The energy curve of the positive-parity state of  $^{28}\text{Ne}$  (figure 1 (b)) has the oblatelly deformed minimum at  $\beta=0.25$  which has a  $0p2h$  structure. We also find the prolately deformed  $2p4h$  structure has a minimum at  $\beta=0.5$  whose energy is about 1MeV above the oblatelly deformed  $0p2h$  state. This small excitation energy of  $2p4h$  structure means that the softness of neutron's  $0d_{3/2}$  orbit again. Since two different structure coexist within the small excitation energy, when we superpose these wave functions, it induces the strong mixing between these configurations which will be discussed in the next subsection. The change of the shape



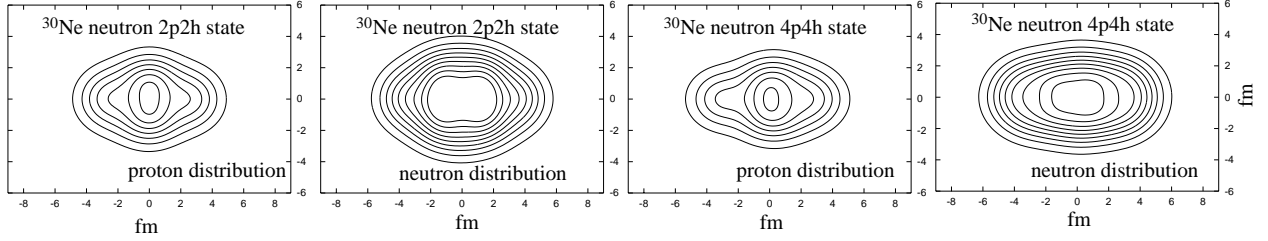


Fig. 3. Proton and neutron intrinsic density distributions of the neutron  $4p4h$  structure of  $^{30}\text{Ne}$ . For the sake of the comparison, those of the  $2p2h$  structure are also shown.

from oblate to prolate is the reason why the single particle energies as functions of  $\beta$  are discontinuous around  $\beta=0.35$  in  $^{28}\text{Ne}$ . The energy of the neutron  $0d_{3/2}$  orbit of  $^{28}\text{Ne}$  becomes lower as deformation becomes larger in the oblately deformed region ( $0 \leq \beta \leq 0.45$ ), while that of  $^{30}\text{Ne}$  (lower  $0d_{3/2}$  of  $^{30}\text{Ne}$ ) which is prolately deformed becomes higher in the region of  $0.1 \leq \beta \leq 0.45$ . These behaviors of the lower  $0d_{3/2}$  orbits are the qualitatively same as those described by the Nilsson model,<sup>30)</sup>  $[N, n_z, m_l, \Omega]=[2, 1, 1, 3/2]$  orbit for the oblate state and  $[N, n_z, m_l, \Omega]=[2, 0, 0, 1/2]$  orbit for the prolate state. Since the neutron number  $N=18$  prefers the oblate deformation in the small deformed region because of the deformed shell effect,  $0p2h$  structure of  $^{28}\text{Ne}$  has a oblate shape. On the contrary, the neutron  $2p4h$  state has a prolate shape because the proton number  $N=10$  prefers the prolate deformation, though the neutron's shell effects are comparable in the prolate and oblate deformation. In this nucleus, the  $4p6h$  structure does not appear as an energy minimum or a shoulder on the energy curve. When we calculate more deformed state, it appears about 20MeV above the  $0p2h$  state and it does not seem to be a stable structure. We think that the absence of the stable  $4p6h$  structure means the hardness of the  $N=16$  deformed shell. Here, by the deformed  $N=16$  shell, we mean a shell of  $sd$  orbits without the orbits coming from the spherical  $d_{3/2}$  orbit.

The energy curve of the positive-parity state of  $^{26}\text{Ne}$  (figure 1 (a)) has an energy minimum at  $\beta=0.25$  which has the  $0p4h$  structure. It also has the  $2p6h$  shoulder in which two neutrons are promoted into  $pf$ -shell, but its excitation energy is rather high (about 7MeV in the case of  $0^+$  state). We note that the  $2p6h$  structure of this nucleus is superdeformed state. The deformed orbit configuration of this state is the same as that of the closed shell state with the magic number of the superdeformation  $N=16$ . However the single-particle energy diagram of figure 2 (a) does not show clearly the deformed magic number  $N=16$ .

Here we make some additional comments on the single particle energy diagrams of Fig.2. Except the oblate region in  $^{28}\text{Ne}$ , the single particle energy diagrams of the three isotopes are very similar to each other. From this similarity we can understand why the deformation of the  $2\hbar\omega$ -jump structure becomes larger for lighter Ne isotope reaching the superdeformation in  $^{26}\text{Ne}$ . It is because the uppermost occupied orbit which crosses first the intruder  $pf$ -orbit

changes to lower  $sd$ -orbit as going to lighter isotope, which results in larger value of  $\beta$  of the crossing point.

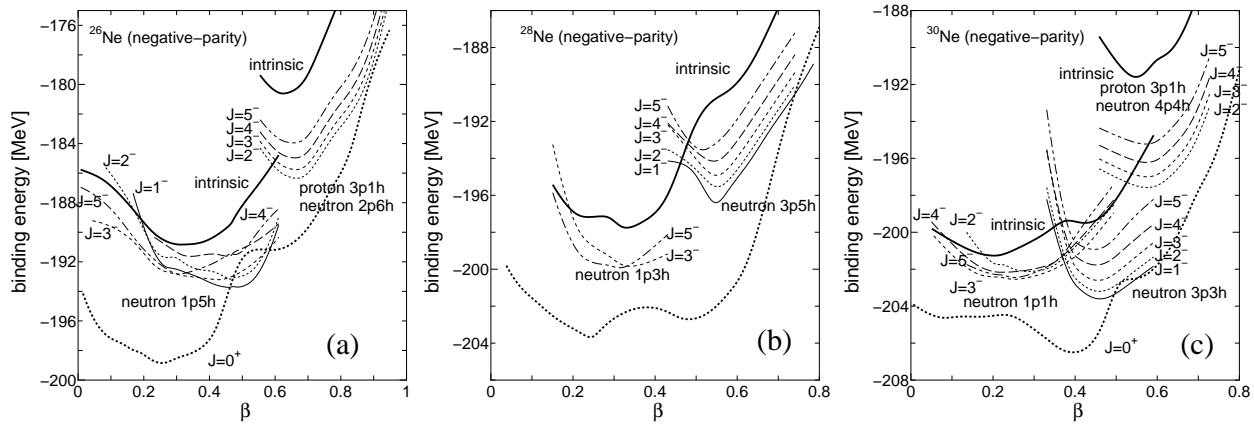


Fig. 4. Obtained energy curves of the negative parity states of  $^{26}\text{Ne}$  (a),  $^{28}\text{Ne}$  (b) and  $^{30}\text{Ne}$  (c). In each panel, the energies of the parity projected intrinsic state (dashed line), the parity and angular momentum projected states are plotted as the functions of the matter quadrupole deformation parameter  $\beta$ .

Next, we discuss the energy curves of the negative-parity states (figure 4). The energy curves of the positive-parity states have shown the softness to excite neutrons in the shell which originates in the spherical  $0d_{3/2}$  shell and the hardness to excite neutrons below  $N=16$ . We find that this feature is inherited in the negative-parity states. Namely, on the one hand the  $1p1h$  and  $3p3h$  structure of  $^{30}\text{Ne}$  and  $1p3h$  structure of  $^{28}\text{Ne}$  have small excitation energies. But on the other hand the  $3p5h$  structure of  $^{28}\text{Ne}$  and  $1p5h$  structure of  $^{26}\text{Ne}$  have larger excitation energies. In the negative-parity states of  $^{30}\text{Ne}$ , there are two low-lying groups of minimums. The curves which are minimized around  $\beta=0.45$  are the  $K^\pi=1^-$  rotational band members which have the  $3p3h$  structure. Around  $\beta=0.3$ , there are  $J^\pi=2^-, 3^-, 4^-$  and  $5^-$  states which have the  $1p1h$  structure. The order of these states are changed by the GCM calculation and will be discussed in the next subsection. The interesting point is that both the  $1p1h$  and  $3p3h$  structure have small excitation energy, 3.6MeV and 4MeV measured from the positive-parity  $2p2h$  state. When we compare the energy curves of the positive- and negative-parity states of  $^{30}\text{Ne}$ , we find that the neutron excitation and nuclear deformation are correlated to each other. As deformation becomes larger, neutrons in the shell which originates in the spherical  $0d_{3/2}$  shell are promoted into  $pf$ -shell, with  $m=0, 1, 2, 3$  and  $4$ , in order for  $mpmh$ . The energy loss due to the neutron promotion is not large and it always comparable with the energy gain due to the deformation of the intrinsic state and the restoration of the rotational symmetry. Thus the neutron  $0-4ph$  structure appears in the low-lying state. It is interesting that the  $J^\pi=1^-$  ( $K^\pi=1^-$ ) state which has a neutron

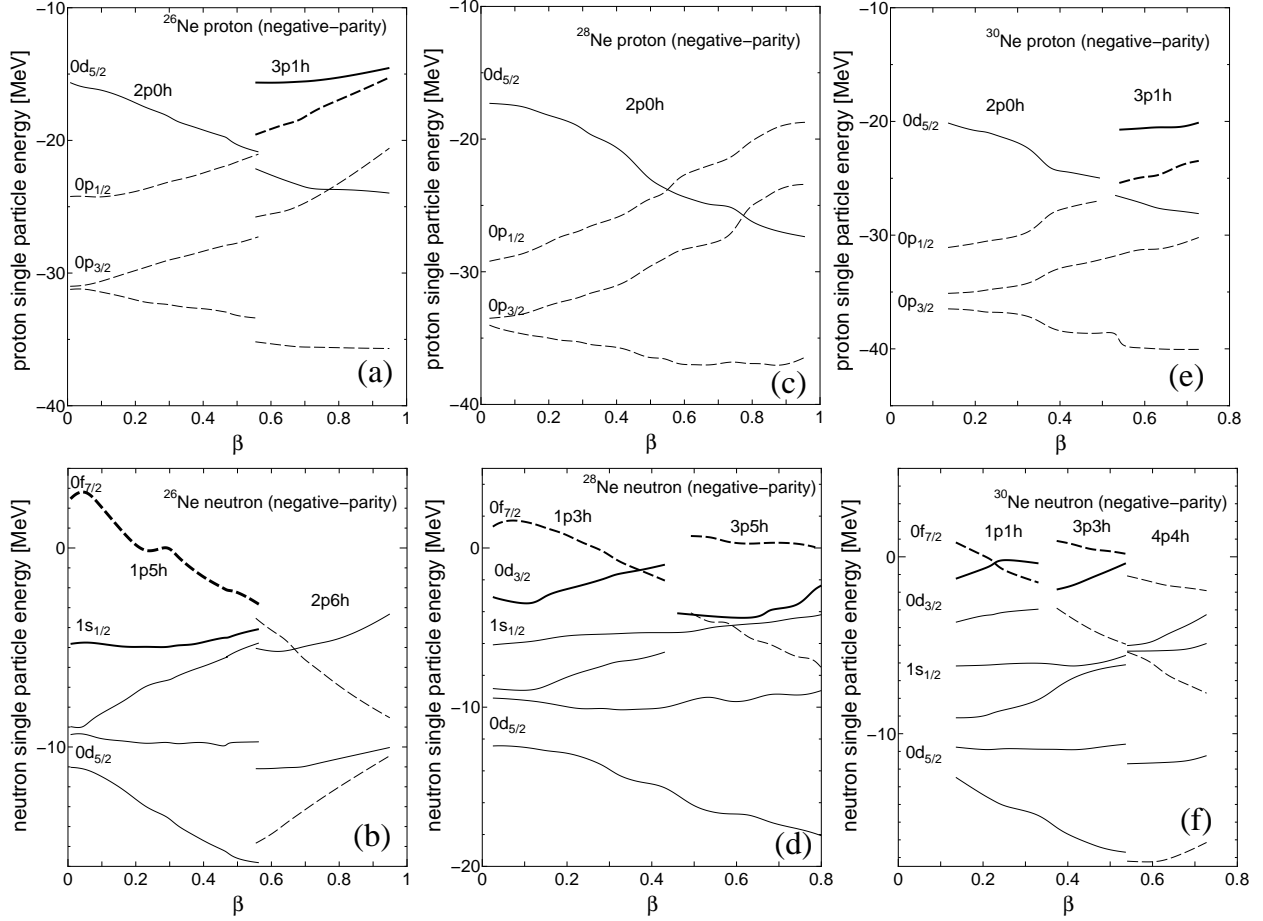


Fig. 5. The proton and neutron single particle energies of  $^{26}\text{Ne}$  (a) (b),  $^{28}\text{Ne}$  (c) (d) and  $^{30}\text{Ne}$  (e) (f) obtained from the intrinsic wave functions on the negative-parity energy curves. The positive (negative) parity single particle orbits are plotted by the solid (dashed) lines. The single particle orbits given by the thin (bold) lines are occupied by two (one) protons or neutrons.

$3p3h$  structure is even lower than the states which has a neutron  $1p1h$  structure. In the shell model calculation,  $1p1h$  structure is lower than the  $3p3h$  structure.<sup>6)</sup> Though the energy loss due to the neutron promotion in the  $3p3h$  structure is larger than the  $1p1h$  structure, larger deformation and smaller angular momentum provide the larger energy gain due to the deformation of the intrinsic state and the restoration of the rotational symmetry. We also find an interesting structure around  $\beta=0.6$  which appears as a  $K^\pi=2^-$  band. Since deformation is too large, neutron  $3p3h$  structure seems to be not able to form a stable mean-field. But neutron  $5p5h$  structure costs much energy because of the hardness of the  $N=16$ . Therefore, a proton in  $0p$ -shell is drafted to make a negative parity state. Namely, in this structure, the system has a proton  $3p1h$  and neutron  $4p4h$  structure in which  $^{16}\text{O}$  core is excited. In other words, this state is understood as the state in which the neutron  $4p4h$  state of the positive-parity state is excited by the proton excitation.

The energy curve of the negative-parity state of  $^{28}\text{Ne}$  has two minima. The lower one which is minimized around  $\beta=0.3$  has a  $1p3h$  structure. It produces  $J=3^-$  and  $5^-$  states and both have small excitation energy. On the contrary, the  $3p5h$  state which produces  $K^\pi=1^-$  band around  $\beta=0.55$  has much larger excitation energy due to the hardness of the deformed  $N=16$  shell. Because of the hardness of the  $N=16$  shell closer, the negative-parity states of  $^{26}\text{Ne}$  do not appear no longer in the low-energy region. It has  $1p5h$  structure around  $\beta=0.5$ , but its energy is about 6MeV higher than the positive-parity  $0p4h$  state. The proton excitation is also found in this nucleus. In the largely deformed region ( $\beta > 0.6$ ), the system chooses the proton  $3p1h$  and neutron  $2p6h$  structure instead of the neutron  $3p7h$  structure. This choice is because of the stability of the superdeformed configuration of neutron.

### 3.2. Low-Lying Level Scheme

After the angular momentum projection, we have superposed the wave functions calculated by the variation and diagonalized (GCM calculation). The obtained level scheme of  $^{26}\text{Ne}$ ,  $^{28}\text{Ne}$  and  $^{30}\text{Ne}$  is shown figure 6. First, we discuss  $^{30}\text{Ne}$ . In the positive-parity state, we have obtained three bands. The ground, second and third bands have dominant contribution from  $2p2h$ ,  $0p0h$  and  $4p4h$  structure, respectively. The mixing between these three neutron configurations is most strong in the  $0^+$  state and becomes smaller as the angular momentum increases.

Similarly to the results of other theoretical studies,  $2_1^+$  state has a small excitation energy (0.88 MeV) and large  $B(E2; 0_1^+ \rightarrow 2_1^+)$  value (table I) due to the dominance of the large deformed  $2p2h$  configuration in the ground band. The mixings between different neutron configurations are weaker in the  $2_1^+$  and  $4_1^+$  states than in the ground state. Therefore the mixing between the neutron configurations lowers the ground state energy than the higher spin states and makes the spectrum of the ground band slightly deviate from the rotational one,  $E(2_1^+)/E(0_1^+)=3.08$ . The second band shows the vibrational spectra. The third band has a  $4p4h$  dominant structure and this band shows the largely deformed rotational spectrum and has large intra-band  $E2$  transition probabilities (table I). Even though we increase the number of the basis states of the GCM calculation, the energy and wave function of the third band is not affected as well as those of the ground

Table I.  $E2$  transition probabilities. Experimental data is taken from Ref.<sup>20)</sup>

	AMD+GCM	EXP
$^{30}\text{Ne}; 0_1^+ \rightarrow 2_1^+$	283	
$0_2^+ \rightarrow 2_2^+$	88	
$0_3^+ \rightarrow 2_3^+$	393	
$^{28}\text{Ne}; 0_1^+ \rightarrow 2_1^+$	208	$269 \pm 136$
$0_1^+ \rightarrow 2_2^+$	112	
$0_2^+ \rightarrow 2_1^+$	109	
$0_2^+ \rightarrow 2_2^+$	239	
$^{26}\text{Ne}; 0_1^+ \rightarrow 2_1^+$	203	$228 \pm 41$
$0_2^+ \rightarrow 2_2^+$	412	

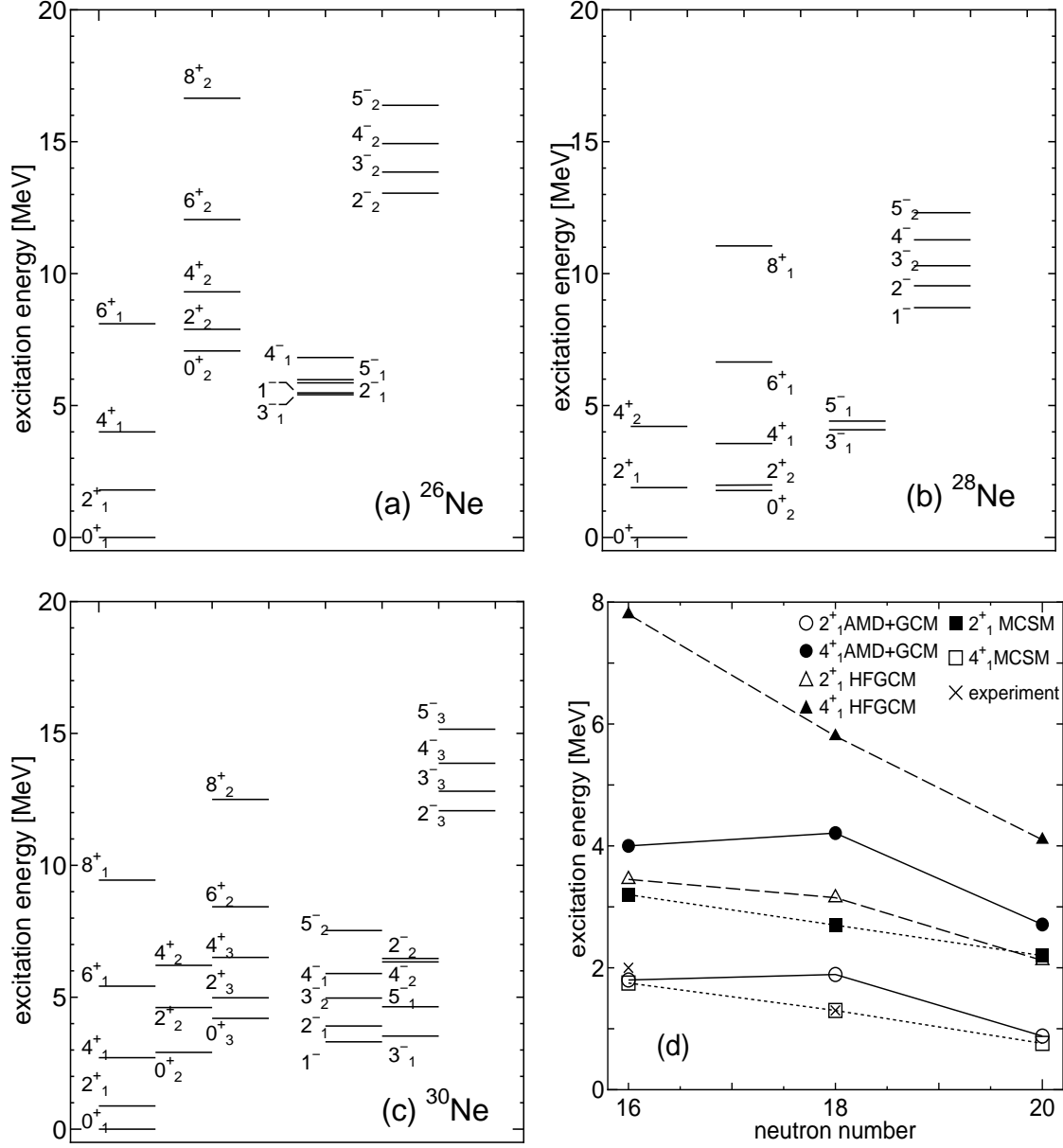


Fig. 6. Calculated low-lying level schemes of (a)  $^{26}\text{Ne}$ , (b)  $^{28}\text{Ne}$  and (c)  $^{30}\text{Ne}$ . (d) shows the comparison of the excitation energies of  $2_1^+$  and  $4_1^+$  states obtained by the present work, the monte carlo shell model<sup>10)</sup> (MCSM), HFB+AMPGCM<sup>17)</sup> and the experiment.

and second bands, and therefore, we consider that this band is stable. The small excitation energy of this band is important, since it means the softness of the neutrons above the deformed  $N=16$  shell. In the same sense, the low-lying negative-parity states are also important, though their spectra are complicated due to a rather strong mixing between  $1p1h$  and  $3p3h$  structures. As discussed in the previous section, due to the large energy gain which owe to the larger deformation and the smaller angular momentum,  $1^-$  state becomes the lowest

negative-parity state.  $3_1^-$  state is lowered by the strong mixing between  $1p1h$  states with the  $3p3h$  structure and in this state,  $1p1h$  structure is dominant, while  $3_2^-$  state becomes higher and have a  $3p3h$  dominant structure.  $5_1^-$  state is also lowered by the mixing between two configurations and in this state, neutron  $1p1h$  structure is dominant. There are not strong mixing between  $2_1^-$  and  $2_2^-$  and between  $4_1^-$  and  $4_2^-$  state and it leaves  $2_2^-$  and  $4_2^-$  states which have  $1p1h$  dominant structure in higher excitation energy than the  $5_1^-$  and  $3_1^-$  states which also have  $1p1h$  structure. The  $K^\pi=2^-$  band in which a proton in  $p$ -shell is excited into  $sd$ -shell combined with the neutron  $4p4h$  structure does not mixed with other states and left in the higher energy region. The obtained low-lying states of  $^{30}\text{Ne}$  have been governed by the neutron's particle-hole configurations. The softness of neutrons in the  $0d_{3/2}$  orbit against the promotion into the  $pf$ -shells produces the low-lying  $0p0h$  and  $2p2h$  rotational bands in  $^{30}\text{Ne}$ . This trend is also common in the case of the negative-parity states. In particular, the lowest negative-parity band,  $K^\pi=1^-$  band which has neutron  $3p3h$  structure dominantly, is as largely deformed as the ground band. And it can be regarded as the  $1\hbar\omega$  excitation from the ground band in the same deformed mean-field as the ground band. The small excitation energy  $K^\pi=0_3^+$  band which has neutron  $4p4h$  structure dominantly can be also regarded as showing the softness of the  $0d_{3/2}$  orbit. However, as is already presented, this band has a ' $\alpha+^{16}\text{O}$ +valance neutrons' type nature like the case of the neutron-rich Be isotopes.<sup>?,31)</sup> It means the coexistence of the deformed mean-field structure and the molecular orbital structure and their interplay which has not clearly seen in the case of the Be isotopes.

The ground band of  $^{28}\text{Ne}$  has a strong mixing between the oblatly deformed  $0p2h$  structure and the prolately deformed  $2p4h$  structure. The mixing is strongest in the case of the  $0^+$  states and it lowers the ground state's energy by about 1.9MeV. This mixing becomes smaller rapidly as the angular momentum becomes larger. As a result, the energy gap between  $0_1^+$  state and  $2_1^+$  state becomes larger and the  $0_1^+$ ,  $2_1^+$  and  $4_1^+$  states of the ground band show vibrational character,  $E_x(4_1^+)/E_x(2_1^+)=2.17$ . The strong mixing also makes the  $E2$  transition probability between the ground state and  $2_1^+$  state smaller compared to that of  $^{30}\text{Ne}$  (table I), since the amount of the largely deformed component becomes smaller than the ground band of  $^{30}\text{Ne}$ . The excitation energy of  $0_2^+$  becomes higher by the mixing. And this is the reason of the small energy gap between  $0_2^+$  and  $2_2^+$  states. In the case of the  $^{30}\text{Ne}$ , the low-lying  $1p1h$  and  $3p3h$  states are mixed strongly. However, in this nucleus, the mixing between  $1p3h$  and  $3p5h$  structure is no longer strong because of their large energy difference. As a result, the  $3_1^-$  and  $5_1^-$  states which have  $1p3h$  structure appears in the lower energy region together with the positive-parity bands, while  $K^\pi=1^-$  band which has  $3p5h$  structure is left in the higher energy region. The softness of neutrons in  $0d_{3/2}$  induces the strong mixing between neutron  $0p2h$  and  $2p4h$  configurations, but the hardness of deformed

neutron N=16 shell makes the mixing between  $1p3h$  and  $3p5h$  state weak.

In the ground band of the  $^{26}\text{Ne}$ , the mixing between the different neutron configurations is much weaker than  $^{30}\text{Ne}$  and  $^{28}\text{Ne}$ . The ground band of the  $^{26}\text{Ne}$  shows a vibrational character,  $E_x(4_1^+)/E_x(2^+)=2.22$ . Due to the hardness of the N=16, neutron  $ph$  states appears more than 5MeV above the ground state. In the positive-parity the superdeformed states which has  $2p6h$  structure appears about 6MeV above the ground state. It seems that the magic number of the superdeformation N=16 which is most detailedly studied in  $^{32}\text{S}$  is still valid even in the neutron-rich region. Indeed, in this superdeformed state, it is possible to excite a proton from  $p$ -shell to  $sd$ -shell by not affecting the stability of this state. This proton excited states appears as the  $K^\pi=2^-$  state in the negative-parity. The lowest negative-parity state is  $3_1^-$  state but its excitation energy is higher than that of the  $^{30}\text{Ne}$  and  $^{28}\text{Ne}$ . Because of the hardness of the deformed neutron N=16 shell, this nucleus does not have any low-lying particle-hole excited states. Instead, it has a superdeformed rotational band about 7MeV above the ground band whose neutron configuration is almost the same as that of the predicted superdeformed state of  $^{32}\text{S}$ .<sup>33),34)</sup> This superdeformed neutron configuration seems to be stable, since it allows the proton excitation within the same superdeformed mean-field which appears as the  $K^\pi=2^-$  band about 13MeV above the ground state.

Finally, we discuss the comparison with the experimental data and the other theoretical results. The excitation energy of  $2_1^+$  state of  $^{26}\text{Ne}$  shows a good agreement with the experiment. However, in our result, the observed  $0_2^+$  state is not obtained. We note that the experimentally observed  $0_2^+$  state at 3.69MeV will not correspond to the  $0_2^+$  state obtained by the present calculation. In the HFB+GCM calculation,<sup>17)</sup> the prolately deformed local minimum which may have a neutron  $0p4h$  structure appears and that will be correspond to the experimentally observed  $0_2^+$  state. Since in the variational calculation, we have made the constraint on the quadrupole deformation parameter  $\beta$ , but not on the  $\gamma$ , we have not obtained the prolately deformed minimum which have neutron  $0p4h$  structure on the energy curve. The excitation energies of  $2_1^+$  and  $4_1^+$  states of  $^{28}\text{Ne}$  and  $^{30}\text{Ne}$  is smaller than those obtained by HFB+GCM calculation<sup>17)</sup> and larger than the monte carlo shell model study<sup>10)</sup> (figure 6 (d)), though the

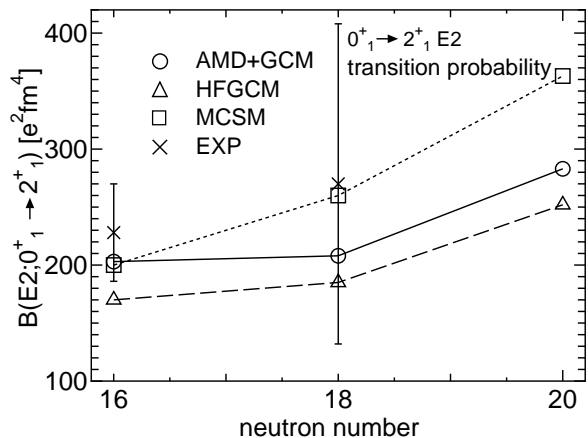


Fig. 7. Calculated and observed  $B(E2; 0_1^+ \rightarrow 2_1^+)$  of Ne isotopes. For comparison, results by monte carlo shell model (MCSM)<sup>10)</sup> and HFB+AMPGCM<sup>17)</sup> are shown.

general trend of these state is common. The difference between our results and HFB+GCM results may be attributed to the difference of the spatial symmetry of the wave function, the difference of the generator coordinates used in the calculation and the lack of the pairing effects in our calculation. However, in the  $B(E2;0_1^+ \rightarrow 2_1^+)$  we do not find such large difference between our results and HFB+GCM results. In  $^{32}\text{Mg}$ , the  $3^-$  state at 2.32 MeV is experimentally proposed,<sup>18),24)</sup> though the assignment of the spin and parity of this state is not still fixed. This state can correspond to the  $3_1^-$  state of  $^{30}\text{Ne}$  at 3.31MeV obtained in the present calculation.

#### §4. Summary

We have studied the low-lying level schemes of  $^{26}\text{Ne}$ ,  $^{28}\text{Ne}$  and  $^{30}\text{Ne}$  using the deformed-basis AMD+GCM method. The obtained energy curves and the level schemes of the positive parity states have shown the softness of the neutrons in the deformed orbits coming from the  $0d_{3/2}$  orbit with respect to the promotion to the  $pf$ -shell and the hardness of neutrons below N=16 deformed shell. The softness leads to the coexistence of the neutron  $0p0h$ ,  $2p2h$  and  $4p4h$  states in  $^{30}\text{Ne}$  and  $0p2h$  and  $2p4h$  states in  $^{28}\text{Ne}$  and to the breaking of the N=20 shell closure in  $^{30}\text{Ne}$ . We also found that this feature is inherited to the negative-parity states. As a result, neutron  $1p1h$  and  $3p3h$  states of  $^{30}\text{Ne}$  and  $1p3h$  state of  $^{28}\text{Ne}$  are predicted to appear in the small excitation energy. We think that the low excitation energies of negative parity states are typical phenomena accompanying the breaking of N=20 shell, but it has not been recognized because almost no theoretical studies including Hartree-Fock approach have been made on negative parity states. The proton excited states in the negative parity states of  $^{30}\text{Ne}$  and  $^{26}\text{Ne}$  which are the results of the hardness of the N=16 deformed shell have been also obtained. The  $\alpha+^{16}\text{O}$  cluster correlations have been noticed to exist in the  $4p4h$  structure of  $^{30}\text{Ne}$ .

#### Acknowledgements

We would like to thank Dr. Y. Kanada-En'yo for valuable discussions. Many of the computational calculations were carried out by SX-5 at Research Center for Nuclear Physics, Osaka University (RCNP). This work was partially performed in the Research Project for Study of Unstable Nuclei from Nuclear Cluster Aspects sponsored by Institute of Physical and Chemical Research (RIKEN).



## References

- 1) I. Tanihata, et. al., Phys. Rev. Lett. **55**, 2676 (1985).
- 2) C. Thibault, R. Klapisch, C. Rigaud, A.M. Poskanzer, R. Prieels, L. Lessard and W. Reisdorf, Phys. Rev. **C 12** 644 (1975).
- 3) X. Campi, H. Flocard, A.K. Kerman, S. Koonin, Nucl. Phys. **A 251**, 193 (1975).
- 4) A. Watt, R. P. Singhal, M. H. Storm and R. R. Whitehead, J. Phys. **G7** L145 (1981).
- 5) A.Poves and J.Retamosa, Phys. Lett. **B184**, 311 (1987).
- 6) E.K.Warburton, J.A.Becker and B.A.Brown, Phys. Rev. **C41**, 1147 (1990).
- 7) N.Fukunishi, T.Otsuka and T.Sebe, Phys.Lett. **B296**, 279 (1992).
- 8) T. Motobayashi, et.al., Phys.Lett. **B346**, 9 (1995).
- 9) D.J.Dean, M.T.Ressell, M.Hjorth-Jensen, S.E.Koonin, K.Langanke and A.P.Zuker, Phys.Rev. **C59**, 2474 (1999).
- 10) Y.Utsuno, T.Otsuka, T.Mizusaki and M.Honma, Phys.Rev. **C60**, 054315 (1999).
- 11) S.Peru, M.Girod and J.F.Berger, Eur.Phys.J. **A9**, 35 (2000).
- 12) M.V.Stoitsov, J.Dobaczewski, P.Ring and S.Pittel, Phys.Rev. **C61**, 034311 (2000).
- 13) R.R.Rodriguez-Guzman, J.L.Egido and L.M.Robledo, Phys.Rev. **C62**, 054319 (2000).
- 14) E.Caurier, F.Nowacki and A.Poves, Nucl.Phys. **A693**, 374 (2001).
- 15) Y.Utsuno, T.Otsuka, T.Mizusaki and M.Honma, Phys.Rev. **C64**, 011301 (2001).
- 16) M.Kimura and H.Horiuchi, Prog.Theor.Phys. **107**, 33 (2002).
- 17) R.R.Rodriguez-Guzman, J.L.Egido and L.M.Robledo, Eur.Phys.J. **A17**, 37 (2003).
- 18) G.Klotz, et.al., Phys.Rev. **C47**, 2502 (1993).
- 19) H. Sakurai, et.al., Phys. Rev. **C54**, R2802 (1996).
- 20) B.V.Pritychenko, et.al., Phys. Lett. **B461**, 322 (1999).
- 21) V. Chiste, et.al., Phys.Lett. **B514**, 233 (2001).
- 22) K. Yoneda, et.al., Phys. Lett. **B499**, 233 (2001).
- 23) F. Azaiez, et.al., Eur. Phys. J. **A15**, 93 (2002).
- 24) W. Mittig, et.al., Prog. Theor. Phys. Suppl. **146** 16, (2002).
- 25) S.Nummela, et.al., Phys. Rev. **C64**, 054313 (2001).
- 26) A. C. Morton, etl.al., Phys. Lett. **B544**, 274 (2002).
- 27) Y.Kanada-En'yo, H.Horiuchi and A.Ono, Phys.Rev. **C52**, 628 (1995).  
Y. Kanada-En'yo, M. Kimura and H. Horiuchi, C.R. Physique **4**, 497 (2003).
- 28) M. Kimura, Phys. Rev. **C**, in print.
- 29) A.Dote, H.Horiuchi and Y.Kanada-En'yo, Phys.Rev. **C56**, 1844 (1997).
- 30) S. G. Nilsson, Mat. Fys. Medd. Dan. Vid. Selsk. bf 29 No. 16., 68 (1955)

- 31) Y.Kanada-Enyo and H.Horiuchi, Prog. Theor. Phys. Suppl. **142**, 205 (2001).
- 32) N. Itagaki, S. Okabe and K. Ikeda, Prog. Theor. Phys. Suppl. **142**, 297 (2001).
- 33) M. Yamagami and K. Matsuyanagi, Nucl. Phys. **A672**, 123 (2000).
- 34) M. Kimura and H. Horiuchi, Phys. Rev. **C**, in print.